Physics of Plasmas

Toward more robust ignition of inertial fusion targets

Cite as: Phys. Plasmas **30**, 022702 (2023); https://doi.org/10.1063/5.0120732
Submitted: 14 August 2022 • Accepted: 30 December 2022 • Published Online: 01 February 2023

J. J. Lee, R. T. Ruskov, H. Martin, et al.

Physics of Plasmas ARTICLE scitation.org/journal/php

Toward more robust ignition of inertial fusion targets

Cite as: Phys. Plasmas **30**, 022702 (2023); doi: 10.1063/5.0120732
Submitted: 14 August 2022 · Accepted: 30 December 2022 ·
Published Online: 1 February 2023

J. J. Lee,[1,a)] R. T. Ruskov,[1] H. Martin,[1] S. Hughes,[1] M. W. von der Layen,[1] R. W. Paddock,[1] R. Timmis,[1] I. Ouatu,[1] Q. S. Feng,[1] S. Howard,[1] E. Atonga,[1] R. Aboushelbaya,[1] T. D. Arber,[2] R. Bingham,[3] and P. A. Norreys[1,4]

AFFILIATIONS

[1]Department of Physics, Atomic and Laser Physics Sub-Department, University of Oxford, Clarendon Laboratory, Parks Road, Oxford OX1 3PU, United Kingdom
[2]Centre for Fusion, Space, and Astrophysics, Department of Physics, University of Warwick, Coventry CV4 7AL, United Kingdom
[3]Central Laser Facility, Rutherford Appleton Laboratory, Didcot, Oxon OX11 0QX, United Kingdom
[4]John Adams Institute for Accelerator Science, University of Oxford, Denys Wilkinson Building, Keble Road, Oxford OX1 3RH, United Kingdom

[a)]Author to whom correspondence should be addressed: jordan.lee@physics.ox.ac.uk

ABSTRACT

Following the 3.15 MJ fusion milestone at the National Ignition Facility, the further development of inertial confinement fusion, both as a source for future electricity generation and for high-energy-density physics applications, requires the development of more robust ignition concepts at current laser facility energy scales. This can potentially be achieved by auxiliary heating the hotspot of low convergence wetted foam implosions where hydrodynamic and parametric instabilities are minimized. This paper presents the first multi-dimensional Vlasov–Maxwell and particle-in-cell simulations to model this collisionless interaction, only recently made possible by access to the largest modern supercomputers. The key parameter of interest is the maximum fraction of energy that can be extracted from the electron beams into the hotspot plasma. The simulations indicate that significant coupling efficiencies are achieved over a wide range of beam parameters and spatial configurations. The implications for experimental tests on the National Ignition Facility are discussed.

I. INTRODUCTION

Fusion energy has the potential to contribute to the rising global energy requirements without negatively impacting the environment.[1,2] The two main approaches to realizing fusion energy are magnetic[3] and inertial[4] confinement fusion. Impressive results have been achieved using both approaches.

Researchers using the Joint European Torus (JET),[5,6] a magnetic confinement fusion (MCF) device, have demonstrated the confinement of a fusion plasma for around 5 s while producing 59 MJ of fusion energy (Q = fusion energy generated/input energy = 0.33). JET's successor, the International Experimental Reactor (ITER),[7] is currently under construction with the aim of surpassing break even and producing 10 times the energy required to heat the plasma ($Q \geq 10$).

For inertial confinement fusion (ICF), recent gains of 1.5 (Q = 1.5) have been reported at the National Ignition Facility (NIF).[8] This is a significant improvement on their previous record of 0.7 achieved in August 2021[9–11] and marks a major milestone in the progress of ICF. The indirect drive approach adopted at the NIF is suitable for achieving their goal of generating a burning plasma.[12]

However, more work is required before inertial fusion energy (IFE) can be considered for commercial use. In particular, this requires the development of robust target designs[13] with significantly larger gains approaching Q = 100. Direct drive ICF offers significantly better hydrodynamic efficiencies and is widely considered to be one of the most promising routes to achieving high-gain ICF implosions. This is largely a result of pioneering work by researchers at the Laboratory for Laser Energetics, University of Rochester, over many decades. The downside, however, is reduced hydrodynamic stability during the implosion.[14] In indirect drive, soft x rays capable of penetrating deeper into the capsule are used to ablate a significant fraction of the capsule's outer layer, thereby mitigating the growth of the Rayleigh–Taylor instability. For direct drive implosions, the use of UV (351 nm) laser

pulses results in a smaller ablation of the outer surface layer of the capsule. This reduced ablation stabilization leads to larger hydrodynamic instability growth and reduced performance.

In 2021, Paddock *et al.*[15] explored directly driven low convergence ratio (low-CR) implosions in which hydrodynamic and parametric instabilities are minimized.[16] They showed that gains of 0.75 ($Q = 0.75$) might be possible using third harmonic light of Nd:glass laser facilities (351 nm) at NIF-scale energies (1.7 MJ). Since then, further work has shown that this gain can be dramatically increased by using deeper UV laser light, for example, 193 nm from ArF excimer lasers or 210 nm fifth harmonic from Nd:glass, and auxiliary heating schemes.[17–21] Here, auxiliary heating refers to a method of depositing additional thermal energy in the hotspot of the compressed fuel before maximum compression. Individually, the impact of both ArF laser pulses and auxiliary heating schemes has been simulated,[20] reporting gains of around 15–17 for a total input of ~2 MJ of energy. They demonstrate that a few kJs of deposited auxiliary heating energy can bring implosions at current facility energy scales (780 kJ, 1.7 MJ) to ignition. By augmenting the gain of robust, low-CR implosions, consistent high-gain implosions can be achieved.

The proposed auxiliary heating scheme is the passing of relativistic electron beams through the central hotspot. It has long been known that electron beams drifting through plasma are able to collectively drive unstable Langmuir waves and collisionlessly exchange energy with plasma electrons.[22–24] Significant theoretical[25,26] and computational[27,28] work has been conducted to study this process due to its wide-ranging applications.[29–32] In the 1970s, models of electron trapping were developed which predict the energy contained in the electric field of the Langmuir waves at the point of saturation.[26,27,33] More recently, work produced by Ratan *et al.*[21] uses relativistic multifluid theory to calculate the initial linear growth rate of the Langmuir waves in the case of electron beams crossed anti-parallel and orthogonally in the case of NIF-relevant implosion hotspots (temperatures of 4 keV and densities of 10^{26} cm^3).

Low-CR implosions are well suited to a heating scheme involving relativistic electron beams, as the larger hotspot associated with these implosions provides a large spatial cross section in which to overlap the beams. In addition, these electron beams are generated using high-intensity, short-pulse lasers incident on the critical density surface of the pre-compressed plasma.[34,35] This method of driving relativistic electron beams of sufficient total energy is similar to that seen in fast ignition ICF.[36,37] However, due to the lower densities and higher temperatures encountered in the hotspot of isobaric implosions, such as those discussed here, the collisional frequency is reduced and collisionless heating is the dominant energy exchange mechanism (in contrast to collisional stopping of fast electrons associated with isochoric implosions for fast ignition).

To make this heating mechanism as attractive as possible, it is crucial to maximize the efficiency of the energy transfer from beam to background electrons in the hotspot. This paper presents possible methods of maximizing this efficiency and is organized as follows. First, the collisionless heating of plasma electrons by anti-parallel relativistic electron beams is presented. Then, models of electron trapping are introduced and the predictions compared to one-dimensional (1D) Vlasov–Maxwell simulations. Three-pulse sequences of electron beams are then assessed over a range of beam temperatures and densities. Two-dimensional and collisional simulations are then presented. Finally, the possibility of a fully robust high-gain target design, the optimization of electron beam generation, and the applicability of auxiliary heating to indirect and direct drive ICF tests are discussed. The simulation results presented in this article required the use of over 1.67×10^6 processor hours, only made possible thanks to the ARCHER2 UK national supercomputing service, which came online at the end of 2021.[38]

II. HEATING MECHANISM

To analyze the heating mechanism, a collisionless, 1D1P (one spatial and one momentum dimension) Vlasov–Maxwell simulation using the VALIS[39–41] code was performed. In this simulation, a background plasma consisting of protons and electrons at 4 keV with electron density $n_e = 0.98\, n_0$, where n_0 is the total electron (and proton) density, was penetrated by two anti-parallel relativistic electron beams. The electron beams had mean kinetic energy, temperature, and density 1 MeV, 40 keV, and $n_b = 0.01\, n_0$, respectively. Figure 1 shows how the energy of the system normalized to the initial kinetic energy of the electron beams developed in time with the key stages of interest labeled. Initially, the electron beams appear as bumps on the tail of the electron distribution function (shown in Fig. 2 at $\omega_p t = 0$) and collisionlessly drive unstable Langmuir waves in the plasma electrons. This is observed between $200\, \omega_p^{-1}$–$300\, \omega_p^{-1}$ as beam electrons lose kinetic energy in the exponential growth of Langmuir waves. The energy contained in these Langmuir waves appears as both electric field energy and the kinetic energy of plasma electrons, leading to the first stage of plasma heating. At $300\, \omega_p^{-1}$, this interaction is saturated and the energy of each component undergoes damped oscillations at the trapping frequency of electrons in the potential well of the dominant Langmuir wave. A secondary heating stage is then observed in which no additional energy is extracted from the electron beam. This heating is due to the release of electric field energy almost entirely into the plasma electron species. In this simulation, the interaction ends at approximately $t = 800\, \omega_p^{-1}$. For a low-CR hotspot with typical densities of 10^{25} cm^{-3} ($\rho = 16.7$ g/cm^3, $M = m_p$), the plasma frequency is $\omega_p = 1.8 \times 10^{17}$ rad/s. This energy exchange therefore takes place over femtosecond timescales. Over the next few picoseconds, collisions will cause the temperature of plasma electrons and protons to equalize.

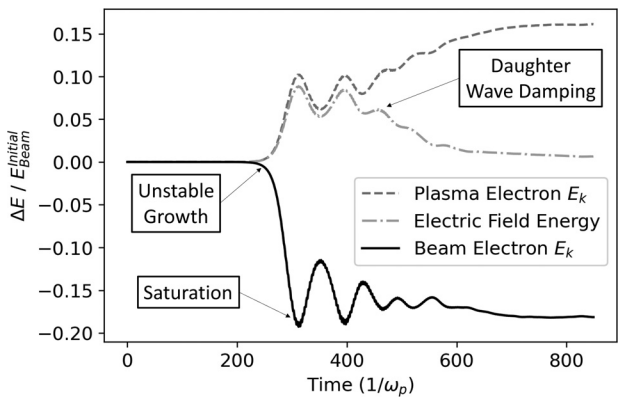

FIG. 1. The kinetic energy of the electron beams (black), kinetic energy of the plasma electrons (dark gray, dashed), and electric field energy (light gray, dash-dotted), all normalized to the initial kinetic energy of the electron beams ($\Delta E / E_{\text{Beam}}^{\text{Initial}}$).

In ICF, the increased temperature of hotspot ions will lead to increased neutron yield.

Studies reported in Refs. 24 and 26–28 have shown that the trapping of beam electrons in the high-intensity Langmuir waves can lead to the saturation of the bump-on-tail instability. This simulation confirms that this is the case for ICF hotspot relevant plasma. Trapping occurs when there is a single dominant Langmuir wave resulting in an almost sinusoidal electric field. In the reference frame of the dominant Langmuir wave, beam electrons travel with a lower velocity. As the amplitude of the electrostatic potential grows exponentially in time, the kinetic energy of the electrons becomes insufficient to overcome the potential barrier. At this point, electrons become trapped and begin to oscillate in the potential, appearing as oscillations in velocity space and rotation in (x, p) phase space. To first confirm that trapping is the dominant saturation mechanism, snapshots of (x, p) phase space are taken at progressive times. As predicted, at the time of saturation ($t = 300\,\omega_p^{-1}$), clear vortices are observed. Beyond this, the beams are smeared in velocity space and appear as plateaus in the electron velocity distribution. This distribution function is purely decreasing, stable, and the bump-on-tail instability is saturated. Figure 2 shows the total electron and plasma electron velocity distribution functions, and Fig. 3 shows the (x, p) phase space of beam electrons at $0\,\omega_p^{-1}$, $300\,\omega_p^{-1}$, $700\,\omega_p^{-1}$, and $1000\,\omega_p^{-1}$.

The secondary stage of heating coincides with the relaxation of the energy stored in the electric field (Fig. 1). This relaxation is due to the Langmuir wave modulational instability (LWMI)[42–45]—similar to the oscillating two-stream instability for electromagnetic pump beams—which is triggered by the presence of a strong electric field with a frequency close to the plasma frequency. The LWMI excites zero-frequency ion density perturbations and daughter Langmuir waves of higher wavenumber (see Fig. 4). The higher wavenumber Langmuir waves correspondingly have lower phase velocities ($p \lesssim m_e c$) than the dominant Langmuir mode ($p \simeq 2.2 m_e c$) and are efficiently Landau damped by thermal plasma electrons. This damping heats up the plasma electrons and results in the formation of suprathermal tails as seen in Fig. 2. By the end of the simulation, almost all of the energy in the electric field has been transferred to the plasma electrons and the secondary stage of heating has been completed.

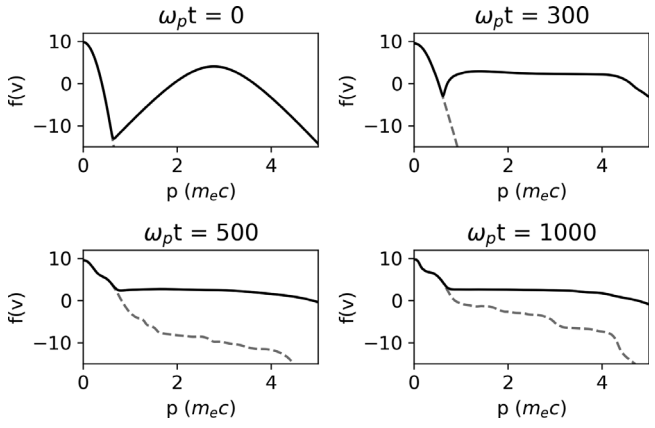

FIG. 2. Total electron distribution function (black) and the plasma electron distribution function (gray, dashed) at $0\,\omega_p^{-1}$, $300\,\omega_p^{-1}$, $500\,\omega_p^{-1}$, and $1000\,\omega_p^{-1}$. Clear steps are generated in the plasma electron distribution function during the second stage of heating ($500\,\omega_p^{-1}$–$1000\,\omega_p^{-1}$) due to the Landau damping of daughter Langmuir waves at decreasing phase velocities.

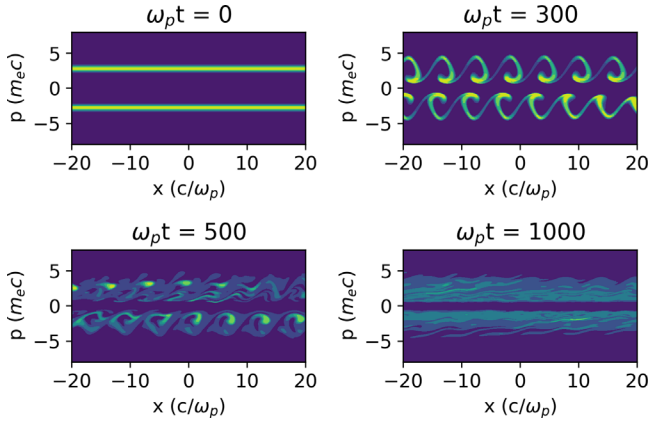

FIG. 3. (x, p) phase space of electron beams at $0\,\omega_p^{-1}$, $300\,\omega_p^{-1}$, $500\,\omega_p^{-1}$, and $1000\,\omega_p^{-1}$. Vortices are formed at $300\,\omega_p^{-1}$ due to trapping of beam electrons in the dominant Langmuir wave.

III. ELECTRON TRAPPING THEORY

Both stages of heating of plasma electrons depend on the electric field energy at saturation. This value normalized to the initial total energy of the electron beams is denoted W (or W_1 if considering the maxima of subsequent oscillations). Models of electron trapping in the relativistic regime show that the dynamics of the interaction are dependent on a single parameter, $S = \beta_0^2 \gamma_0 (\frac{n_b}{2n_0})^{\frac{1}{3}}$, where $\beta_0 = v_b/c$ and $\gamma_0 = (1 - \beta_0^2)^{-\frac{1}{2}}$ are the usual relativistic quantities of the beam electrons.[27,45]

Quasi-linear analysis by Fainberg *et al.*[46] assumes a broad wave spectrum in k-space and shows that the saturation amplitude is given by

$$W = 0.158S. \tag{1}$$

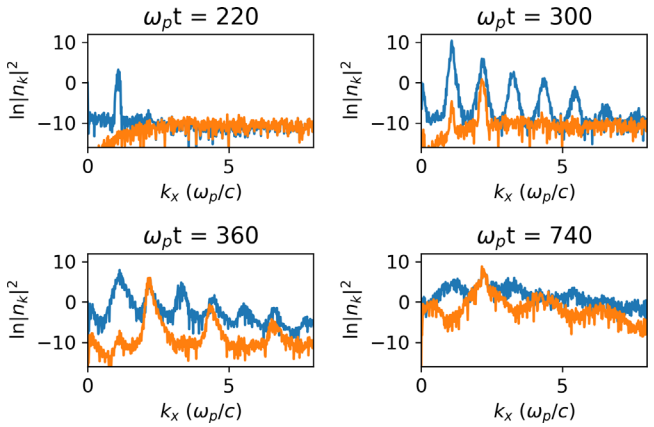

FIG. 4. Spatial Fourier transform showing the generation of daughter Langmuir (blue) and ion acoustic (orange) waves. These waves have lower phase velocities than the dominant Langmuir wave and are efficiently Landau damped.

A similar expression is obtained by Kovtun and Rukhadze[47] who assume a narrow wave spectrum and approximate this by a single, large-amplitude wave.

For cold (beam temperature $= T_b = 0$), relativistic electron beams, a semi-quantitative model developed by Thode and Sudan[33,45,48] predicts that the saturation amplitude of the electric field energy is given by

$$2W = S(1+S)^{-\frac{5}{2}}. \tag{2}$$

This model also uses the single-wave approximation and relaxes the assumption that beam electrons rigidly rotate in (x, p) phase space. Due to the exponential increase in the wave amplitude, the majority of the energy extracted from the beam occurs in the last few e-folds. Therefore, it is assumed that the amplitude reaches its saturation value suddenly. This model takes into account the change in energy of the electron beam due to smearing in momentum space, whereas the rigid rotator model only accounts for the energy change associated with the shift in mean drift energy. Since the change in energy due to smearing in momentum space only becomes appreciable for values of $S \gtrsim 1$, this model may not accurately predict the coupling efficiency for lower values of S.

These models also predict that, during the first heating stage, approximately half of the energy extracted from the beam is absorbed in the oscillatory motion of the plasma electrons, and the other half in the form of the electric field energy of the wave. This is supported by simulation results and can be observed in Fig. 1. Together with the assumption that, during the second stage of heating, all electric field energy is released entirely into the plasma electrons, the total heating of plasma electrons can be estimated by $2W$. Equation (1) can then be used to predict the coupling efficiency of the interaction in the low S regime, and Eq. (2) can be used for larger values. A maximum coupling efficiency of $2W_{\max} = 0.186$ (18.6% coupling efficiency) can then be obtained from Eq. (2) when $S_{\max} = 2/3$.

IV. SIMULATION RESULTS

A. 1D parameter scans

To test the validity of the electron trapping models, a series of VALIS simulations using a range of beam energies and densities are run. Since S is only dependent on beam velocity (energy) and density, these simulations verify the models' predictive capabilities over both parameters. A total of 25 simulations were run and are arranged into three sets. The first set consists of 15 simulations in which the beam density is fixed to $n_b = 0.01 n_0$ and the beam energy is varied from 0.15 to 8 MeV. In the second and third set, consisting of five simulations each, the beam energy is fixed to 1 and 2 MeV, respectively, and the beam density is varied from $n_b = 0.005\, n_0$ to $n_b = 0.04\, n_0$. Combined, these simulations cover values of S ranging from 0.09 to 2.83. Figure 5 plots the coupling efficiencies found in these simulations against the curves predicted by Eqs. (1) and (2). A table containing the temperature increase in the plasma electrons along with some additional simulation input parameters is added in the supplementary material to supplement this figure.

The simulations directly output the kinetic energy of each species, so the total change in energy of the electron beams can then be found by comparing the initial kinetic energy to the final kinetic energy $\Delta E = E_k^{\text{Initial}} - E_k^{\text{final}}$. To directly compare the simulation results with the theoretical models, this change in energy must be normalized to the initial total energy of the electron beams. This is obtained by multiplying the kinetic energy coupling efficiency, $\tilde{W}$, directly obtained from the simulation outputs, by a prefactor of $(\gamma_0 - 1)/\gamma_0$.

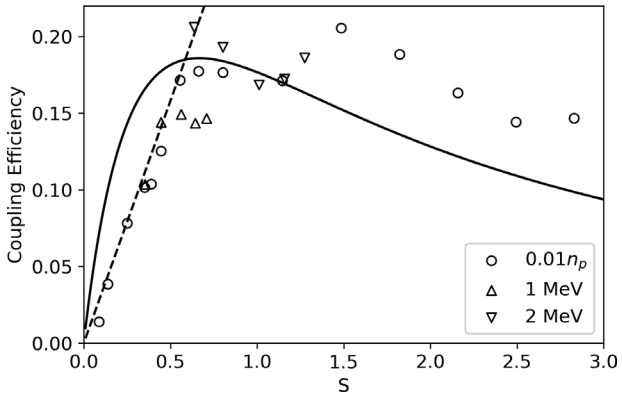

FIG. 5. Coupling efficiency of the beam–plasma interaction as a function of S for three sets of simulations. Set 1 ($0.01\, n_p$) has constant density, $n_p = 0.01\, n_0$, and varied energy, $0.15\,\text{MeV} \leq E \leq 8\,\text{MeV}$. Sets two (1 MeV) and three (2 MeV) have constant energies of 1 and 2 MeV, respectively, and the beam densities are varied from $0.005\, n_0$ to $0.04\, n_0$. These values are compared to those predicted by electron trapping theory given by Eq. (1) (dotted) and Eq. (2) (solid).

$$2W = \frac{\gamma_0 - 1}{\gamma_0} 2\tilde{W} = \frac{\gamma_0 - 1}{\gamma_0} \frac{\Delta E}{E_k^{\text{Initial}}}. \tag{3}$$

It is worthwhile noting that, although run for over $2500\omega_p^{-1}$, the first two simulations of the energy parameter scan (0.15 and 0.25 MeV) did not complete the second phase of heating. The decay of electric field energy in these simulations is significantly lower than for the higher S electron beams as the amplitude of the dominant Langmuir wave is too low to effectively drive the Langmuir wave modulational instability. Regardless, the majority of heating still occurs in these simulations and only about 10% of the total energy remains in the form of electric field energy that has yet to decay.

The simulation results fit well with the quasi-linear model for $S \leq 0.5$. For values of S above this, the approximations used in the quasi-linear model break down and the coupling efficiency is better described by Eq. (2). In the high-energy regime ($S \geq 1.5$), the coupling efficiency deviates from the predicted values. This is due to additional energy being extracted from the electron beams after the first oscillation. The electron trapping models predict the first minimum in beam energy. As shown in Fig. 1, for a beam with strength $S = 0.45$, the first minimum in beam energy is the global minimum and is approximately equal to the final coupling efficiency. For stronger beams, the global minimum does not coincide with the first minimum. Instead, additional energy is extracted from the beams during the oscillatory period. The electric field energy of the consecutive minima, W_1, W_2, W_3, and W_4, is given in Fig. 2(b) of Ref. 27. For $S \geq 1$, the global minimum occurs at the fourth oscillation and has a similar trend to the results shown in Fig. 5. For the purposes of auxiliary heating discussed in this paper, the key finding of this parameter scan is that for $S \gtrsim 0.6$, the coupling efficiency plateaus to approximately 15%–20%.

B. Three-pulse simulations

There is no plasma temperature dependence in Eqs. (1) and (2). This implies that a hotspot that has once been heated could be further heated by applying additional electron beam pulses without decreasing

the beam-plasma coupling efficiency. This would also imply that a hotspot that has been pre-heated by fast electrons before a "main pulse" would still be heated with significant coupling efficiencies. During the process of generating a main electron beam pulse, it is likely that some fast electrons would be generated beforehand. The robustness of this heating scheme to hotspot pre-heating can be studied by considering a sequence of electron beam pulses. This multi-beam approach is simulated using a sequence of VALIS simulations. The plasma temperature after heating in a first simulation is recorded and used as an initial condition for a subsequent simulation in which a second electron beam is applied. This is repeated for a total of three electron beam pulses for a variety of electron beam densities and temperatures ranging from $0 < n_b/n_0 < 0.04$ and $20\,\text{keV} < T_b < 170$ keV, respectively. The energy of all beams used in these simulations is 1 MeV. Figure 6(a) shows the three heating stages for electron beams with temperature 50 keV. The final plasma temperature increases, and the three-beam averaged coupling efficiency is displayed in Figs. 6(b) and 6(c). For the two sparsest beams, with $n_b/n_0 = 0.005$ and 0.01, the heating is seen to be largely independent of the beam temperature, maintaining an overall fractional temperature increase in around 3 and 5, respectively. For the higher density beams, it is apparent that lower beam temperatures give rise to more significant heating. The higher efficiencies reported for the more dense beams can be explained using Eq. (2). It has been shown that the maximum value of W is given for $S = 2/3$. For these 1 MeV beams, $n_b/n_0 = 0.01$ gives $S = 0.45$, whereas $n_b/n_0 = 0.04$ gives $S = 0.71$. It is clear from this that the optimum value of S is approached for increasing densities, hence larger predicted coupling efficiencies. However, for higher energy electron beams, this is not the case. Instead, the lower density beams have larger predicted coupling efficiencies. Therefore, these simulations indicate that optimizing S by varying the energy of the electron beams while remaining in the low-density regime ($n_b < 0.02\,n_0$) will ensure that there is little temperature dependence on the coupling efficiency. It is worthwhile noting that Eq. (2) is restricted to the case where $n_b/n_0 \ll 1$ and may not describe the higher density beams as accurately. Figure 6(a) shows that the heating (and efficiency) becomes somewhat diminished for the second and third pulses. Interestingly, this efficiency decrease only occurs between the first and second pulses as the second and third pulses have similar efficiency values. Ultimately, the averaged three-pulse efficiency remains above 8% across the entire parameter scan.

C. 2D simulations

The simulations discussed previously were one-dimensional. To confirm no higher dimensional effects limit the coupling efficiency, 2D simulations were conducted. These simulations also allowed the angle between the electron beams to be varied and thus the impact of this to be investigated. The relativistic multifluid theory discussed in Ref. 21 predicts a higher linear growth rate of the dominant Langmuir wave when the electron beams are crossed orthogonally. These simulations are able to test whether this corresponds to an increased saturation electric field energy and, hence, coupling efficiency. Vlasov–Maxwell codes are notoriously processor-intensive, so, due to the high cost of 2D simulations, only the orthogonal beam case is simulated using VALIS. To supplement this simulation, additional particle-in-cell simulations using EPOCH[49] are used to simulate both the anti-parallel and orthogonal beam cases in 2D and are compared to the Vlasov simulation. In the 2D orthogonal beam case, an additional drift is added to the plasma electrons to ensure there is no net current. The results from these simulations show close agreement and are depicted in Fig. 7. Although numerical heating inherent to low-resolution simulations is present in

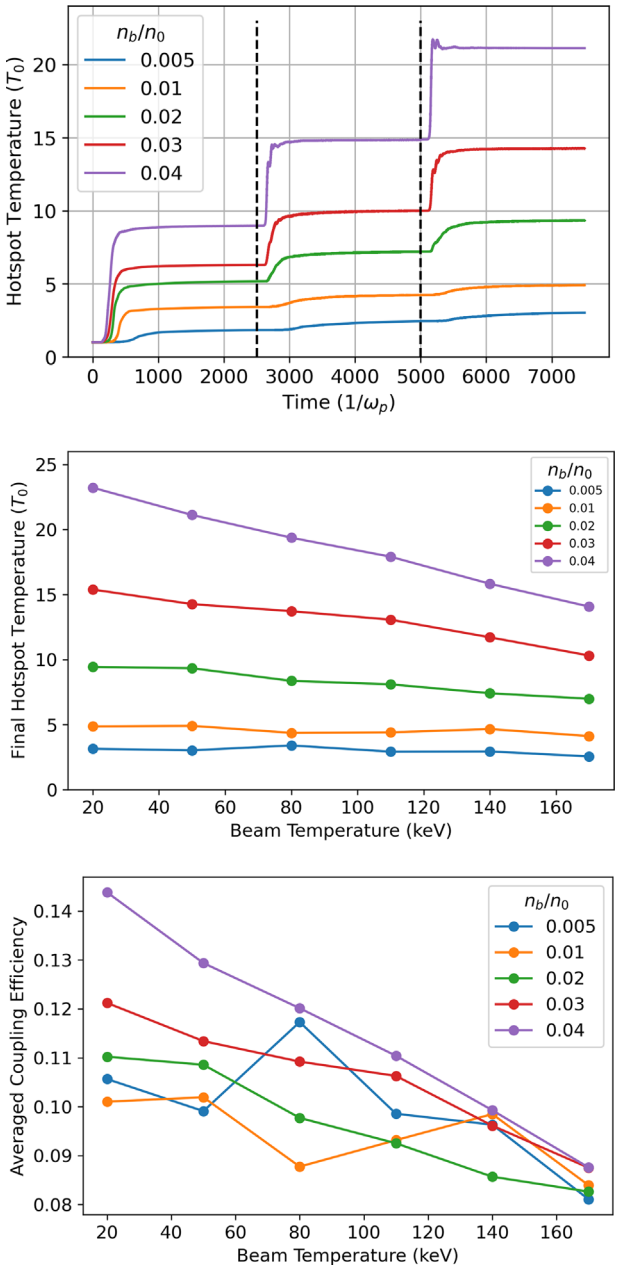

FIG. 6. (a) Temperature evolution of the plasma electrons normalized to the initial temperature, $T_0 = 4$ keV, for a sequence of three electron beams with a temperature of 50 keV. (b) Final hotspot temperature of all three pulse simulations. There is no temperature dependence for low-density beams ($n_b = 0.005\,n_0$, $0.01\,n_0$). For higher density beams, the coupling efficiency increases with decreasing beam temperatures. (c) Averaged three-pulse coupling efficiency for all three pulse simulations.

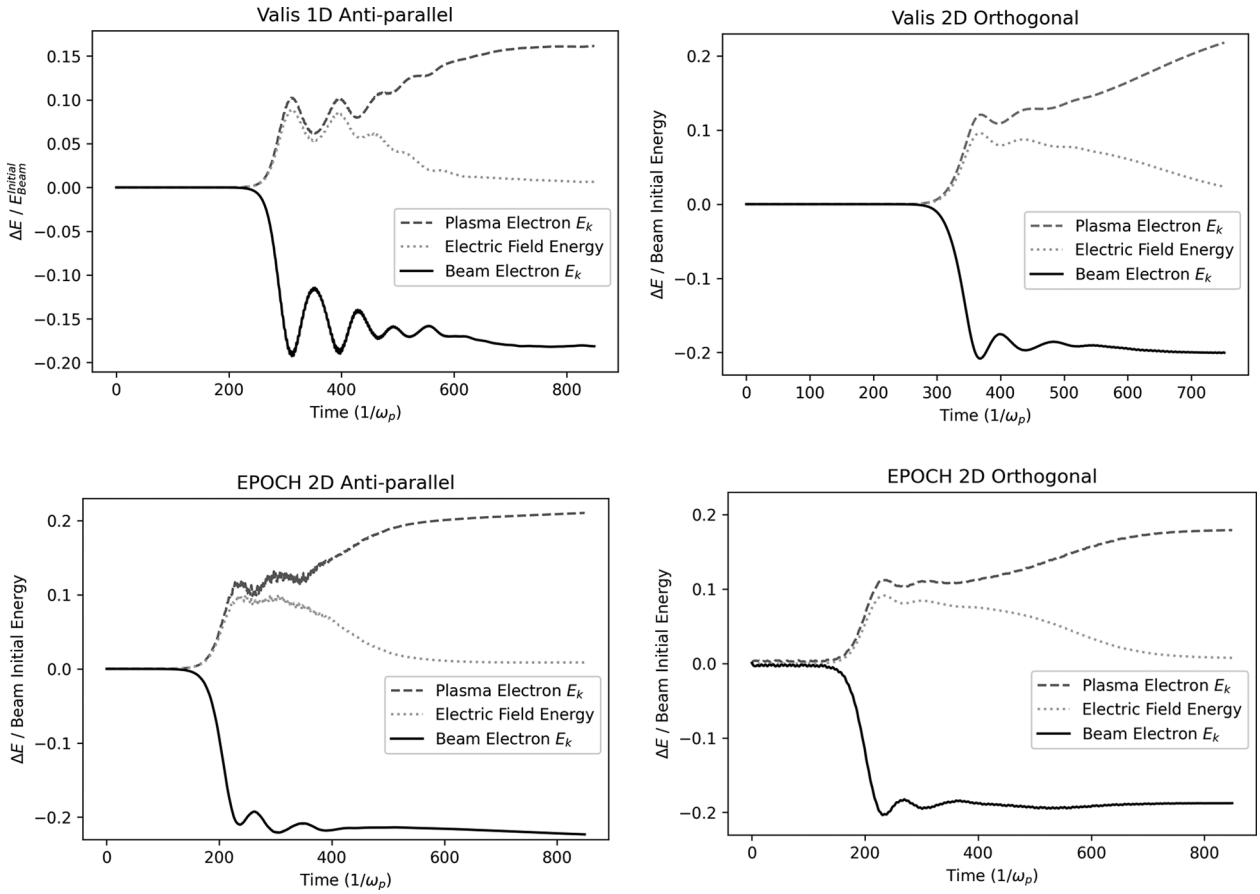

FIG. 7. 2D simulation results for electron beams with energy and density 1 MeV and $n_b/n_0 = 0.01$. Results show no decreased coupling efficiency for electron beams crossed anti-parallel or orthogonally.

the plasma electron species of the 2D VALIS simulation, the coupling efficiencies calculated from the beam electron species are consistent across all simulations. The only discrepancy between the 1D and 2D simulations in both EPOCH and VALIS is the amplitude of the oscillations after saturation. These oscillations are significantly reduced in the 2D case due to the spread of electron trajectories transverse to the dominant Langmuir wave. These results lead to the conclusion that 2D effects do not limit the coupling efficiency of the interaction and that crossing the beams orthogonally, instead of anti-parallel, has little impact. This latter point is more significant than may be apparent when considering the practical application of this heating mechanism. In the anti-parallel case, electron beams will be driven into the optical devices used to generate the opposite electron beam and can lead to damage. In addition, further physical benefits are noted when considering the filamentation and hosing of these electron beams in the plasma.[28,35,50]

One additional 2D EPOCH simulation is run in which the electron beams are crossed at an angle of 5°. At such shallow angles, it is possible that the two overlapping beams act similarly to a single beam with double the density. In this case, it is hard to define the strength of the electron beams. If the electron beams act independently, the strength of the interaction is $S = 0.45$ with a predicted coupling efficiency of $2W = 0.14$ (14%). If the electron beams can instead be considered as a single beam of double density, the beam strength is $S = 0.56$ giving $2W = 0.18$ (18%). This simulation gives insight into how these beams interact. A coupling efficiency of 18.6% is measured from this simulation. This implies that beams overlapping at narrow angles do not act independently. Further simulations with varied beam angles are required to fully understand the transition from independent to interacting electron beams.

D. Collisional simulation

Finally, a 1D EPOCH simulation involving a collision operator is used to confirm that collisions do not inhibit the generation of the primary Langmuir waves in fusion-relevant conditions. Collisions act as a damping mechanism for plasma waves and may be strong enough to stop the generation of the primary Langmuir waves from the bump-on-tail instability. With a plasma density of $10^{25}\,\mathrm{cm}^{-3}$ at 4 keV, the plasma frequency is over a hundred times the electron collisional frequency. It is therefore reasonable to assume that collisions will have little impact on this collisionless exchange process. Simulation results indeed corroborate this reasoning as the simulation was unaffected by

collisions. Provided collisions do not inhibit the collisionless energy exchange, their presence may, instead, increase the coupling efficiency. The small number of collisions that will occur allows for an additional mechanism for beam electrons to deposit energy in the hotspot plasma. This collisional energy exchange may be further enhanced once the collisionless heating has saturated and lowered the mean energy of the beam electrons. The lower energy beam electrons will be more susceptible to collisions and may deposit additional energy deeper into the hotspot (Refs. 51–53).

V. DISCUSSION

A. Robust heating scheme

The results from the one-dimensional simulations show significant coupling efficiencies for a wide range of beam parameters. For strong ($S \geq 0.6$), low-density ($n_b \leq 0.02\, n_0$) electron beams, coupling efficiencies of 15%–20% are achieved and can be expected to be largely independent of beam temperature. These are promising results, as significant heating occurs over a wide range of parameters that are experimentally difficult to control, lessening the need for precise manipulation of the implosion. The robustness of this heating scheme lends itself nicely to augmenting low-CR implosions. Together, there is potential for a fully robust, high-gain target design to be explored.

B. Optimizing electron beam generation

Due to the parallels with fast ignition, significant work has been done to optimize the generation of the electron beams used in this heating scheme. In particular, this involves depositing the laser energy as close to the hotspot as possible. This can be achieved using the radiation pressure of high-intensity lasers to push the critical density surface of the plasma. This mechanism is referred to as hole boring.[54,55] In these high laser intensity regimes, the penetration depth of the laser pulse is further increased via relativistic induced transparency[56] and relativistic self-focusing.[57] For more information on low-density channel formation, hole boring, self-focusing, and relativistic transparency, see Ref. 57 and the references therein. It has been shown that highly collimated hot electron pulses are generated along the laser axis during this intense laser–plasma interaction.[58] The three-pulse simulations indicate that heating from electrons generated during the channeling period will not significantly reduce the efficiency of the primary electron pulse.

Tonge *et al.*[59] have simulated the interaction of intense ($I > 10^{19}$ W/cm^2) laser pulses incident on a steep density gradient overdense plasma. Such a density profile can be generated using the previously mentioned mechanisms. Results show that approximately 80% of the absorbed laser energy is carried by electrons with energy $\leq$3 MeV, ideal for this heating scheme. Taking into account collisions in the highly overdense plasma region surrounding the hotspot, lower energy electrons, which are more susceptible to collisions, will be scattered out of the fast electron spectrum. This results in a lower velocity spread, high-energy "beam-like" distribution. Tonge *et al.* further show that the total fraction of laser energy absorbed by the dense core is around 15%. Another study[60] has found a larger fraction of absorbed energy above 50%. Using these efficiencies combined with a 17% coupling efficiency from fast electrons to plasma electrons, final coupling efficiencies of 2.5% and 8.5% are obtained.

C. Applicability to indirect drive ICF tests

This heating mechanism can be utilized in both direct and indirect drive ICF hotspot implosions. Simulations using Prism Computational Sciences' VISRAD thermal radiation code[61] show that modifying the hohlraum used in indirect drive experiments[69,70] to include holes in the side does not lead to significantly reduced irradiance on the surface of the capsule and only marginally affects the symmetry of the implosion. This comparison can be made between Figs. 8 and 9. Figure 8 shows that the holes provided by this "rugby ball"-shaped hohlraum allow for the auxiliary heating laser beams to irradiate the plasma near these new petawatt laser entrance holes. At this

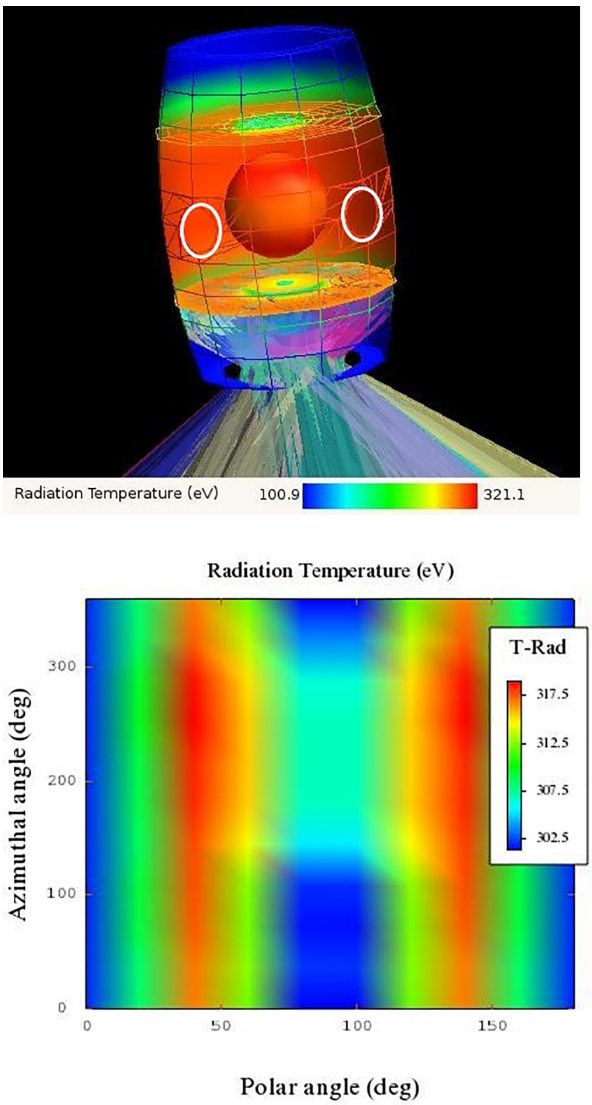

FIG. 8. (a) shows the hohlraum temperature at 0.5 ns for a "rugby ball"-shaped hohlraum with petawatt laser entrance holes. All 192 NIF laser beams are used (image only displays laser pulses entering the hohlraum through the bottom). The entrance is outlined in white for clarity. (b) shows the temperature distribution on the surface of the capsule.

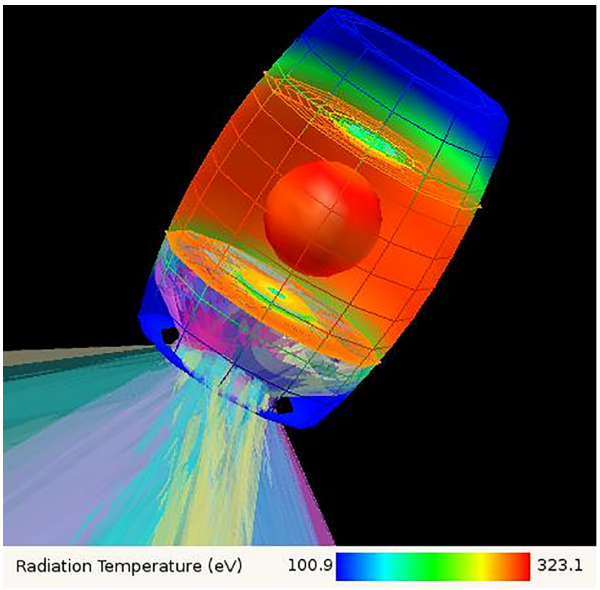

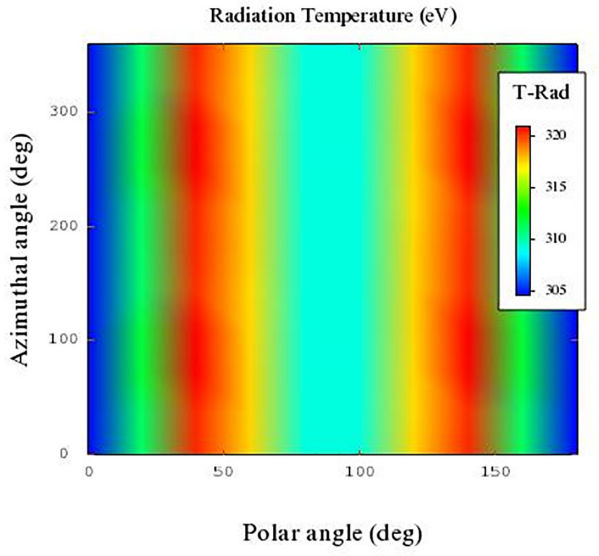

FIG. 9. (a) shows the hohlraum temperature at 0.5 ns for a rugby ball-shaped hohlraum without petawatt laser entrance holes. All 192 NIF laser beams are used (image only displays laser pulses entering the hohlraum through the bottom). (b) shows the temperature distribution on the surface of the capsule.

density, the Habara–Kodama–Tanaka whole-beam self-focusing mechanism[62] guides the petawatt pulses toward the compressed core.[55] This work provides a novel route to testing the physics of auxiliary heating on the largest scale (i.e., the National Ignition Facility).[63–66] In particular, the short-pulse NIF-ARC laser[67,68] can be utilized to generate the relativistic electron beams. Although the simulation results reporting high gains in Ref. 20 are direct drive, the yield amplification due to auxiliary heating can still be tested on indirect drive facilities at reduced scale as simulated in Ref. 17. If the energy supplied by the NIF-ARC laser were to be increased to 100 kJ, the total output energy could be double the 1.3 MJ result reported in August 2021.[20] One notes that the combined direct-drive compression (OMEGA 60) and petawatt (OMEGA EP) facility can also be utilized for these purposes, along with the GEKKO XII and LFEX facilities at Osaka University.[62]

VI. CONCLUSION

The collisionless heating of plasma electrons due to relativistic electron beams has been described, and models of electron trapping have been used to predict the fraction of energy extracted from the electron beams. One-dimensional simulations show good agreement with electron trapping theory and indicate coupling efficiencies of $\sim$17% for strong ($S \geq 0.6$), low-density ($n_b \leq 0.02\, n_0$) electron beams. Two-dimensional and collisional simulations show this coupling efficiency is not reduced by higher dimensional effects or the damping associated with collisions. This auxiliary heating scheme can be used on both direct and indirect drive laser facilities where the increase in gain can be tested. There is potential for this heating scheme to be used to augment low-convergence wetted foam implosions to produce robust high-gain target designs for inertial fusion energy applications (Refs. 69 and 70).

SUPPLEMENTARY MATERIAL

See the supplementary material for details of the simulation codes used and the data required to recreate the results. Tabulated values of the results shown in Fig. 5 are also given.

ACKNOWLEDGMENTS

The authors thank the staff at the UKRI-STFC Rutherford Appleton Laboratory for their assistance in running simulations on the SCARF Supercomputer and the ARCHER2 support team for their help using the ARCHER2 National Supercomputer under Grant Nos. UKRI-EPSRC e674 and EP/R029148/1. R.A., Q.S.F., and P.A.N. were supported by the Oxford-ShanghaiTech agreement. M.W.L. is funded via UKRI-STFC Grant No. ST/T001933/1. The authors gratefully acknowledge support from the John Adams Institute under UKRI-STFC Grant No. ST/V001655/1.

AUTHOR DECLARATIONS

Conflict of Interest

The authors have no conflicts to disclose.

Author Contributions

Jordan John Lee produced simulation results and wrote the manuscript. Heath Martin produced three-pulse simulation results. Rusko Todorov Ruskov provided vital discussion regarding electron trapping theory. Stephen Hughes provided simulation results of modified hohlraum designs. All the authors discussed the results. Peter Norreys supervised the project.

Jordan John Lee: Data curation (lead); Formal analysis (lead); Investigation (lead); Visualization (lead); Writing – original draft (lead); Writing – review & editing (equal). **Sunny Howard:** Writing – review & editing (supporting). **Eduard Atonga:** Writing – review & editing (supporting). **Ramy Aboushelbaya:** Supervision (supporting).

Tony D. Arber: Supervision (equal); Validation (equal); Writing – review & editing (equal). **R. Bingham:** Writing – review & editing (equal). **Peter Norreys:** Conceptualization (lead); Project administration (lead); Supervision (lead); Validation (lead); Writing – original draft (supporting); Writing – review & editing (equal). **Rusko Todorov Ruskov:** Formal analysis (equal); Investigation (equal); Writing – original draft (supporting); Writing – review & editing (equal). **Heath Martin:** Data curation (supporting); Formal analysis (supporting); Investigation (supporting); Visualization (supporting). **Stephen Hughes:** Data curation (supporting); Formal analysis (supporting); Investigation (supporting); Visualization (supporting). **Marko von der Leyen:** Supervision (equal); Validation (equal). **Robert Paddock:** Validation (supporting); Writing – review & editing (equal). **Robin Timmis:** Validation (supporting); Writing – review & editing (supporting). **Iustin Ouatu:** Writing – review & editing (supporting). **Qingsong Feng:** Writing – review & editing (equal).

DATA AVAILABILITY

The data that support the findings of this study are available within the article and its supplementary material.

REFERENCES

[1]L. J. Perkins, "The role of inertial fusion energy in the energy marketplace of the 21st century and beyond," Nucl. Instrum. Methods Phys. Res. A **415**, 44–60 (1998).

[2]K. Tokimatsu, J. Fujino, Y. Asaoka, Y. Ogawa, K. Okano, T. Yoshida, R. Hiwatari, S. Konishi, S. Nishio, K. Yamaji, and Y. Kaya, "Studies of nuclear fusion energy potential based on a long-term world energy and environment model," in *The 18th International Atomic Energy Agency Fusion Energy Conference*, Sorrento, Italy, 4–10 October 2000 (IAEA, 2001), https://www-pub.iaea.org/mtcd/publications/pdf/csp_008c/html/node352.htm.

[3]C. Huang and L. Li, "Magnetic confinement fusion: A brief review," Front. Energy **12**, 305–313 (2018).

[4]S. Jacquemot, "Inertial confinement fusion for energy: Overview of the ongoing experimental, theoretical and numerical studies," Nucl. Fusion **57**, 102024 (2017).

[5]E. Gibney, "Nuclear-fusion reactor smashes energy record," Nature **602**, 371 (2022).

[6]X. Litaudon, S. Abduallev, M. Abhangi, P. Abreu, M. Afza, K. M. Aggarwal, T. Ahlgren, J. H. Ahn, L. Aho-Mantila, N. Aiba *et al.*, "Overview of the JET results in support to ITER," Nucl. Fusion **57**, 102001 (2017).

[7]B. Bigot, "Progress toward ITER's first plasma," Nucl. Fusion **59**, 112001 (2019).

[8]See https://www.energy.gov/articles/doe-national-laboratory-makes-history-achieving-fusion-ignition for an overview of the 1.35 MJ implosion at the NIF (2022).

[9]H. Abu-Shawareb, R. Acree, P. Adams, J. Adams, B. Addis, R. Aden, P. Adrian, B. B. Afeyan, M. Aggleton, L. Aghaian *et al.*, "Lawson criterion for ignition exceeded in an inertial fusion experiment," Phys. Rev. Lett. **129**, 075001 (2022).

[10]A. B. Zylstra, A. L. Kritcher, O. A. Hurricane, D. A. Callahan, J. E. Ralph, D. T. Casey, A. Pak, O. L. Landen, B. Bachmann, K. L. Baker *et al.*, "Experimental achievement and signatures of ignition at the National Ignition Facility," Phys. Rev. E **106**, 025202 (2022).

[11]A. L. Kritcher, A. B. Zylstra, D. A. Callahan, O. A. Hurricane, C. R. Weber, D. S. Clark, C. V. Young, J. E. Ralph, D. T. Casey, A. Pak *et al.*, "Design of an inertial fusion experiment exceeding the Lawson criterion for ignition," Phys. Rev. E **106**, 025201 (2022).

[12]A. B. Zylstra1, O. A. Hurricane1, D. A. Callahan, A. L. Kritcher, J. E. Ralph, H. F. Robey, J. S. Ross, C. V. Young, K. L. Baker, D. T. Casey *et al.*, "Burning plasma achieved in inertial fusion," Nature **601**, 542–548 (2022).

[13]J. Tollefson, "Exclusive: Laser-fusion facility heads back to the drawing board," Nature **608**, 20–21 (2022).

[14]V. A. Smalyuk, C. R. Weber, O. L. Landen, S. Ali, B. Bachmann, P. M. Celliers, E. L. Dewald, A. Fernandez, B. A. Hammel, G. Hall *et al.*, "Review of hydrodynamic instability experiments in inertially confined fusion implosions on National Ignition Facility," Plasma Phys. Controlled Fusion **62**, 014007 (2020).

[15]R. W. Paddock, H. Martin, R. T. Ruskov, R. H. H. Scott, W. Garbett, B. M. Haines, A. B. Zylstra, R. Aboushelbaya, M. W. Mayr, B. T. Spiers, R. H. W. Wang, and P. A. Norreys, "One-dimensional hydrodynamic simulations of low convergence ratio direct-drive inertial confinement fusion implosions," Philos. Trans. R. Soc. A **379**, 20200224 (2021).

[16]B. M. Haines, R. E. Olson, W. Sweet, S. A. Yi, A. B. Zylstra, P. A. Bradley, F. Elsner, H. Huang, R. Jimenez, J. L. Kline *et al.*, "Robustness to hydrodynamic instabilities in indirectly driven layered capsule implosions," Phys. Plasmas **26**(1), 012707 (2019).

[17]P. A. Norreys, L. Ceurvorst, J. D. Sadler, B. T. Spiers, R. Aboushelbaya, M. W. Mayr, R. Paddock, N. Ratan, A. F. Savin, R. H. W. Wang *et al.*, "Preparations for a European R&D roadmap for an inertial fusion demo reactor," Philos. Trans. R. Soc. A **379**, 20200005 (2021).

[18]P. A. Norreys, C. Ridgers, K. Lancaster, M. Koepke, and G. Tynan, "Prospects for high gain inertial fusion energy: An introduction to the second edition," Philos. Trans. R. Soc. A **379**, 20200028 (2021).

[19]P. Norreys, "Auxiliary heating of inertial confinement fusion targets," Bull. Am. Phys. Soc. **59**, 7 (2014).

[20]R. W. Paddock, H. Martin, R. T. Ruskov, R. H. H. Scott, W. Garbett, B. M. Haines, A. B. Zylstra, E. M. Campbell, T. J. B. Collins, R. S. Craxton *et al.*, "Pathways towards break even for low convergence ratio direct-drive inertial confinement fusion," J. Plasma Phys. **88**(3), 905880314 (2022).

[21]N. Ratan, N. J. Sircombe, L. Ceurvorst, J. Sadler, M. F. Kasim, J. Holloway, M. C. Levy, R. Trines, R. Bingham, and P. A. Norreys, "Dense plasma heating by crossing relativistic electron beams," Phys. Rev. E **95**, 013211 (2017).

[22]F. F. Chen, *Introduction to Plasma Physics and Controlled Fusion* (Springer International Publishing, Cham, 2016), Chap. 6.6, 7.4, and 7.5.

[23]V. N. Tsytovich, *Nonlinear Effects in Plasma* (Plenum, New York, 1970).

[24]C. J. Rapson, "Numerical and experimental investigation of beam-plasma-instabilities," Ph.D. thesis (Ernst-Moritz-Arndt-Universität, 2012).

[25]S. A. Bludman, K. M. Watson, and M. N. Rosenbluth, "Statistical mechanics of relativistic streams—II," Phys. Fluids **3**, 747 (1960).

[26]W. E. Drummond, J. H. Malmberg, T. M. O'Neil, and J. R. Thompson, "Nonlinear development of the beam-plasma instability," Phys. Fluids **13**, 2422 (1970).

[27]M. Lampe and P. Sprangle, "Saturation of the relativistic two-stream instability by electron trapping," Phys. Fluids **18**, 475–481 (1975).

[28]A. Bret, L. Gremillet, and M. E. Dieckmann, "Multidimensional electron beam-plasma instabilities in the relativistic regime," Phys. Plasmas **17**, 120501 (2010).

[29]D. J. Hoarty, S. F. James, H. Davies, C. R. D. Brown, J. W. O. Harris, C. C. Smith, S. J. Davidson, E. Kerswill, B. J. B. Crowley, and S. J. Rose, "Heating of buried layer targets by 1ω and 2ω pulses using the HELEN CPA laser," High Energy Density Phys. **3**, 115 (2007).

[30]G. Sarri, K. Poder, J. M. Cole, W. Schumaker, A. Di Piazza, B. Reville, T. Dzelzainis, D. Doria, L. A. Gizzi, G. Grittani *et al.*, "Generation of neutral and high-density electron-positron pair plasmas in the laboratory," Nat. Commun. **6**, 6747 (2015).

[31]M. Tabak, J. Hammer, M. E. Glinsky, W. L. Kruer, S. C. Wilks, J. Woodworth, E. M. Campbell, M. D. Perry, and R. J. Mason, "Ignition and high gain with ultrapowerful lasers," Phys. Plasmas **1**, 1626 (1994).

[32]H. Shiraga, H. Nagatomo, W. Theobald, A. A. Solodov, and M. Tabak, "Fast ignition integrated experiments and high-gain point design," Nucl. Fusion **54**, 054005 (2014).

[33]L. E. Thode and R. N. Sudan, "Two-stream instability heating of plasmas by relativistic electron beams," Phys. Rev. Lett. **30**, 732 (1973).

[34]A. P. L. Robinson, D. J. Strozzi, J. R. Davies, L. Gremillet, J. J. Honrubia, T. Johzaki, R. J. Kingham, M. Sherlock, and A. A. Solodov, "Core electrons and specific heat capacity in the fast electron heating of solids," Nucl. Fusion **54**, 054003 (2014).

[35]A. J. Kemp, F. Fiuza, A. Debayle, T. Johzaki, W. B. Mori, P. K. Patel, Y. Sentoku, and L. O. Silva, "Laser-plasma interactions for fast ignition," Nucl. Fusion **54**, 054002 (2014).

[36]C. Deutsch, "Fast ignition schemes for inertial confinement fusion," Eur. Phys. J. Appl. Phys. **24**, 95–113 (2003).
[37]N. J. Sircombe, R. Bingham, M. Sherlock, T. Mendonça, and P. Norreys, "Plasma heating by intense electron beams in fast ignition," Plasma Phys. Controlled Fusion **50**, 065005 (2008).
[38]See https://www.archer2.ac.uk/ for details of the ARCHER2 national supercomputer.
[39]N. J. Sircombe and T. D. Arber, "Valis: A split-conservative scheme for the relativistic 2D Vlasov-Maxwell system," J. Comput. Phys. **228**, 4773–4788 (2009).
[40]C. Z. Cheng and G. Knorr, "The Integration of the Vlasov equation in configuration space," J. Comput. Phys. **22**, 330 (1976).
[41]P. Colella and P. R. Woodward, "The piecewise parabolic method (PPM) for gas-dynamical simulations," J. Comput. Phys. **54**, 174 (1984).
[42]K. Papadopoulos, "Nonlinear stabilization of beam plasma interactions by parametric effects," Phys. Fluids **18**, 1769–1777 (1975).
[43]M. J. Everett, A. Lal, C. E. Clayton, W. B. Mori, C. Joshi, and T. W. Johnston, "Coupling between electron plasma waves in laser-plasma interactions," Phys. Plasmas **3**, 2041 (1996).
[44]J. T. Mendonca, P. Norreys, R. Bingham, and J. R. Davies, "Beam instabilities in laser-plasma interaction: Relevance to preferential ion heating," Phys. Rev. Lett. **94**, 245002 (2005).
[45]L. E. Thode and R. N. Sudan, "Plasma heating by relativistic electron beams—I: Two-stream instability," Phys. Fluids **18**, 1552 (1975).
[46]Y. B. Fainberg, V. Shapiro, and V. Shevchenko, "Nonlinear theory of interaction between a monochromatic beam of relativistic electrons and a plasma," Sov. Phys. JETP **30**, 528 (1970).
[47]R. I. Kovtun and A. A. Rukhadze, "Nonlinear interaction of a low-density relativistic electron beam with a plasma," Zh. Eksp. Teor. Fiz. **58**, 1709 (1970).
[48]L. E. Thode, "Energy lost by a relativistic electron beam due to two-stream instability," Phys. Fluids **19**, 305–315 (1976).
[49]T. D. Arber, K. Bennett, C. S. Brady, A. Lawrence-Douglas, M. G. Ramsay, N. J. Sircombe, P. Gillies, R. G. Evans, H. Schmitz, A. R. Bell, and C. P. Ridgers, "Contemporary particle-in-cell approach to laser-plasma modeling," Plasma Phys. Controlled Fusion **57**, 113001 (2015).
[50]J. M. Hill, M. H. Key, S. P. Hatchett, and R. R. Freeman, "Beam-Weibel filamentation instability in near-term and fast-ignition experiments," Phys. Plasmas **12**, 082304 (2005).
[51]A. R. Bell, J. R. Davies, S. Guerin, and H. Ruhl, "Fast-electron transport in high-intensity short-pulse laser - solid experiments," Plasma Phys. Controlled Fusion **39**, 653 (1997).
[52]S. Atzeni, A. Schiavi, and J. Davies, "Stopping and scattering of relativistic electron beams in dense plasmas and requirements for fast ignition," Plasma Phys. Controlled Fusion **51**, 015016 (2008).
[53]A. Solodov and R. Betti, "Stopping power and range of energetic electrons in dense plasmas of fast-ignition fusion targets," Phys. Plasmas **15**, 042707 (2008).
[54]S. C. Wilks, W. L. Kruer, M. Tabak, and A. B. Langdon, "Absorption of ultra-intense laser pulses," Phys. Rev. Lett. **69**, 1383 (1992).
[55]A. J. Kemp and L. Divol, "Interaction physics of multipicosecond petawatt laser pulses with overdense plasma," Phys. Rev. Lett. **109**, 195005 (2012).
[56]V. Vshivkova, N. Naumovab, F. Pegoraroc, and S. Bulanov, "Nonlinear interaction of ultra-intense laser pulses with a thin foil," Phys. Plasmas **5**, 2727 (1998).
[57]B. T. Spiers, M. P. Hill, C. Brown, L. Ceurvorst, N. Ratan, A. F. Savin, P. Allan, E. Floyd, J. Fyrth, L. Hobbs *et al.*, "Whole-beam self-focusing in fusion-relevant plasma," Philos. Trans. R. Soc. A **379**, 20200159 (2020).
[58]A. L. Lei, A. Pukhov, R. Kodama, T. Yabuuchi, K. Adumi, K. Endo, R. R. Freeman, H. Habara, Y. Kitagawa, K. Kondo *et al.*, "Relativistic laser channeling in plasmas for fast ignition," Phys. Rev. E **76**, 066403 (2007).
[59]J. Tonge, J. May, W. B. Mori, F. Fiuza, S. F. Martins, R. A. Fonseca, L. O. Silva, and C. Ren, "A simulation study of fast ignition with ultrahigh intensity lasers," Phys. Plasmas **16**, 056311 (2009).
[60]D. J. Strozzi, M. Tabak, D. J. Larson, L. Divol, A. J. Kemp, C. Bellei, M. M. Marinak, and M. H. Key, "Fast-ignition transport studies: Realistic electron source, integrated particle-in-cell and hydrodynamic modeling, imposed magnetic fields," Phys. Plasmas **19**(7), 072711 (2012).
[61]J. J. MacFarlane, "VISRAD-A 3-D viewfactor code and design tool for high-energy density physics experiments," J. Quant. Spectrosc. Radiat. Transfer **81**, 287–300 (2003).
[62]T. Gong, H. Habara, K. Sumioka, M. Yoshimoto, Y. Hayashi, S. Kawazu, T. Otsuki, T. Matsumoto, T. Minami, K. Abe *et al.*, "Direct observation of imploded core heating via fast electrons with super-penetration scheme," Nat. Commun. **10**, 5614 (2019).
[63]H. S. Park, O. A. Hurricane, D. A. Callahan, D. T. Casey, E. L. Dewald, T. R. Dittrich, T. Döppner, D. E. Hinkel, L. F. B. Hopkins, S. L. Pape *et al.*, "The high velocity, high adiabat, 'Bigfoot' campaign and tests of indirect-drive implosion scaling," Phys. Rev. Lett. **112**, 055001 (2014).
[64]E. I. Moses, J. D. Lindl, M. L. Spaeth, R. W. Patterson, R. H. Sawicki, L. J. Atherton, P. A. Baisden, L. J. Lagin, D. W. Larson, B. J. MacGowan *et al.*, "Overview: Development of the national ignition facility and the transition to a user facility for the ignition campaign and high energy density scientific research," Fusion Sci. Technol. **69**(1), 1–24 (2016).
[65]M. L. Spaeth, K. R. Manes, D. H. Kalantar, P. E. Miller, J. E. Heebner, E. S. Bliss, D. R. Spec, T. G. Parham, P. K. Whitman, P. J. Wegner *et al.*, "Description of the NIF laser," Fusion Sci. Technol. **69**(1), 25–145 (2016).
[66]M. L. Spaeth, K. R. Manes, M. Bowers, P. Celliers, J. M. D. Nicola, P. D. Nicola, S. Dixit, G. Erbert, J. Heebner, D. Kalantar, O. Landen, B. MacGowan, B. Van Wonterghem, P. Wegner, C. Widmayer, and S. Yang, "National ignition facility laser system performance," Fusion Sci. Technol. **69**(1), 366–394 (2016).
[67]C. P. J. Barty, M. Key, J. Britten, R. Beach, G. Beer, C. Brown, S. Bryan, J. Caird, T. Carlson, and J. Crane, "An overview of LLNL high-energy short-pulse technology for advanced radiography of laser fusion experiments," Nucl. Fusion **44**, S266 (2004).
[68]J. K. Crane, G. Tietbohl, P. Arnold, E. S. Bliss, C. Boley, G. Britten, G. Brunton, W. Clark, J. W. Dawson, and S. Fochs, "Progress on converting a NIF quad to eight, petawatt beams for advanced radiography," J. Phys.: Conf. Ser. **244**, 032003 (2010).
[69]R. E. Olson, L. J. Suter, J. L. Kline, D. A. Callahan, M. D. Rosen, S. N. Dixit, O. L. Landen, N. B. Meezan, J. D. Moody, C. A. Thomas *et al.*, "X-ray conversion efficiency in vacuum hohlraum experiments at the National Ignition Facility," Phys. Plasmas **19**, 053301 (2012).
[70]R. E. Olson, M. J. Schmitt, B. M. Haines, G. E. Kemp, C. B. Yeamans, B. E. Blue, D. W. Schmidt, A. Haid, M. Farrell, P. A. Bradley, H. F. Robey, and R. J. Leeper, "A polar direct drive liquid deuterium-tritium wetted foam target concept for inertial confinement fusion," Phys. Plasmas **28**, 122704 (2021).